INSTITUTE OF PHYSICS PUBLISHING PLASMA SOURCES SCIENCE AND TECHNOLOGY
Plasma Sources Sci. Technol. **11** (2002) 413–425 PII: S0963-0252(02)39781-0

Slow wave ion heating in the HELIX helicon source

J L Kline, E E Scime, R F Boivin, A M Keesee and X Sun

Physics Department, West Virginia University, Morgantown, WV 26505, USA

E-mail: escime@wvu.edu

Received 29 April 2002, in final form 10 July 2002
Published 24 September 2002
Online at stacks.iop.org/PSST/11/413

Abstract
Ion temperature measurements have been made at multiple axial and radial locations in a helicon source for a range of magnetic field strengths and RF frequencies. The observed temperature gradient along the axis suggests limited thermal transport along the magnetic field. The radial profiles are flat near the axis and in some cases peak near the edge of the plasma. The ion temperature measurements combined with calculations of the perpendicular wave numbers for the slow wave or 'Trivelpiece–Gould' mode are consistent with ion heating due to ion Landau damping of the slow wave at the edge of the plasma.

1. Introduction

Helicon sources are constructed for a wide variety of purposes, e.g. plasma processing studies [1–5], plasma thruster development [6, 7], basic plasma physics experiments [8–11], and space relevant plasma physics experiments [10, 12, 13]. However, there are many fundamental aspects about how helicon sources operate that are not well understood. The wide range of construction characteristics along with the wide range of operating parameters hinders the development of a comprehensive theoretical model explaining helicon source operation. One feature lacking in typical theoretical models is ion motion effects [14, 15], even though experimental evidence suggests that ions could play an important role [16, 17]. Ion motion effects are ignored in such models by assuming the RF frequency is much greater than the lower hybrid frequency. Therefore, ion motion effects are especially important for helicon sources that operate near the lower hybrid frequency [18].

The only published theoretical treatment of helicon sources that includes ion motion effects on fast and slow wave propagation is the work of Cho [19]. However, singularities in the equations forced him to use rough approximations in his zeroth-order calculations. Another limitation of Cho's, and some other cold plasma dielectric treatments, is the use of uniform plasma densities to avoid the difficulties associated with a radially varying dielectric tensor. Since no existing model of wave excitation and damping in helicon sources includes all of the effects that experiments suggest are important, the predictions of the different models have to be carefully considered in light of the assumptions used in the calculations. Even when calculations include ion motion effects, the ions are assumed to exist at room temperature (0.02 eV) and only introduce small corrections to the dielectric tensor. To the best of our knowledge, there are no theoretical calculations that have examined the possible effects of 0.75 eV ions on wave propagation and RF power absorption in helicon plasmas.

In this work, a simple free space, cold plasma model [19] for a helicon source is used to calculate the perpendicular wave numbers for the slow wave ('Trivelpiece–Gould' mode) and the fast wave ('Helicon' mode) near the lower hybrid frequency. The simple model is described in section 2 and the effects of the neutral pressure, plasma density, parallel wave number, wave frequency, and magnetic field strength on the perpendicular wave numbers of the slow wave are investigated. The experimental apparatus is described in section 3 and ion temperature measurements, that show a clear correlation with the local lower hybrid frequency, are presented in section 4. In section 5, the ion temperature measurements are discussed in terms of the model and a mechanism for ion heating, ion Landau damping of slow waves at the edge of the plasma, is proposed. Edge ion heating and the dependence of the ion temperature on particular values of magnetic field strength and RF frequency are just two of the pieces of evidence that will be presented in support the slow wave damping hypothesis. The implications of these experimental measurements and some

conclusion about helicon source operation are presented in section 6.

2. Theory

Solving the cold plasma dispersion relationship including ion terms and collisions, Cho [19] found two solutions for typical helicon operating parameters. The first solution is that of the fast, or helicon, wave (a bounded, right circularly polarized electromagnetic, whistler wave). Experimental measurements confirm that electromagnetic waves with wave fields consistent with helicon waves propagate downstream of the RF antenna in helicon sources [20, 21]. The second solution is the slow wave or 'Trivelpiece–Gould' mode. The slow wave is a surface wave and is heavily damped by collisions, preventing it from propagating towards the centre of the plasma [22]. Near the lower hybrid resonance, the slow wave becomes almost completely electrostatic. Attempts to directly measure the slow wave in a helicon plasma source have been hampered by the extremely short wavelength of the slow wave, $\lambda \sim 1$ mm. Density profile measurements [23] have provided preliminary but not conclusive evidence of slow wave excitation in helicon sources. Ion heating measurements [17], along with recent high-frequency current measurements [24], provide the first clear experimental evidence of slow wave excitation in helicon sources.

The cold plasma dispersion relation, including ion motion effects and collisions, for typical helicon source plasma parameters is [19]

$$\rho^4 - (\alpha + \beta)\rho^2 + \alpha\beta - \gamma\delta = 0, \tag{1}$$

where $\rho = k_\perp c/\omega$ and α, β, γ, and δ are

$$\alpha = \varepsilon_1 - N^2 - \frac{\varepsilon_2^2}{\varepsilon_1}, \tag{2}$$

$$\beta = \varepsilon_3\left(1 - \frac{N^2}{\varepsilon_1}\right), \tag{3}$$

$$\gamma = \frac{N\varepsilon_3\varepsilon_2}{\varepsilon_1}, \tag{4}$$

$$\delta = \frac{N\varepsilon_2}{\varepsilon_1}, \tag{5}$$

$N = k_{||}c/\omega$, $k_\perp$ is the perpendicular wave number, and $k_{||}$ is the parallel wave number. ε_1, ε_2, and ε_3 are the elements of the cold plasma dielectric tensor:

$$\varepsilon_1 = 1 + \sum_{j=e,i} \frac{\omega_{pj}^2(1 + i\nu_j/\omega)}{\omega_{cj}^2 - \omega^2(1 + i\nu_j/\omega)^2}, \tag{6}$$

$$\varepsilon_2 = \sum_{j=e,i} \frac{\sigma_j\omega_{pj}^2(\omega_{cj}/\omega)}{\omega_{cj}^2 - \omega^2(1 + i\nu_j/\omega)^2}, \tag{7}$$

$$\varepsilon_3 = 1 - \sum_{j=e,i} \frac{\omega_{pj}^2}{\omega^2(1 + i\nu_j/\omega)^2}, \tag{8}$$

where j represents quantities of the jth species, ω_{cj} is the cyclotron frequency, ω_{pj} is the plasma frequency, ν_j is the total collision frequency, and σ_j is the sign of the charge. Near the lower hybrid resonance,

$$\frac{1}{\omega_{lh}^2} = \frac{1}{\omega_{ce}\omega_{ci}} + \frac{1}{\omega_{pi}^2 + \omega_{ci}^2}, \tag{9}$$

or when ε_1 goes to zero, the perpendicular wave number of the slow wave goes to infinity for a collisionless plasma. The collision term, which includes ion–ion, electron–electron, ion–neutral and electron–neutral collisions, reduces the perpendicular wave number of the slow wave at the lower hybrid resonance to a finite value and, for large collision frequencies, slightly shifts the resonant frequency.

The perpendicular wave number versus magnetic field strength obtained from the cold plasma dispersion relation is shown in figure 1 for an argon plasma (argon is used for all calculations). At low magnetic fields, there is only one solution to the dispersion relation. As the magnetic field strength increases, the single solution bifurcates into the fast and slow waves. For the fast, helicon, wave solution, the perpendicular wave number decreases asymptotically to zero for large magnetic fields. The perpendicular wave number of the fast wave also varies smoothly near the lower hybrid frequency. For the slow wave solution, the perpendicular wave number increases to infinity (in a collisionless plasma) when the wave frequency equals the lower hybrid frequency, i.e. the lower hybrid resonance. The corresponding perpendicular phase speed, $\omega/k_\perp$, of the slow wave goes to zero. If the wave phase speed becomes comparable to the ion thermal speed, $k_\perp v_{thi}/\omega \sim 1$, ion Landau damping can occur [25]. The potential for large perpendicular wave numbers suggests that the Landau damping of the slow wave could explain the large perpendicular ion temperatures observed in helicon sources operating near the lower hybrid frequency [16]. Note that although the imaginary component of the slow wave is shown as positive in figure 1, it is the absolute value of the imaginary component that is graphed. In fact, the slow wave is strongly damped (imaginary part < 0) at the lower hybrid resonance ($B \sim 850$ G). Most helicon experiments

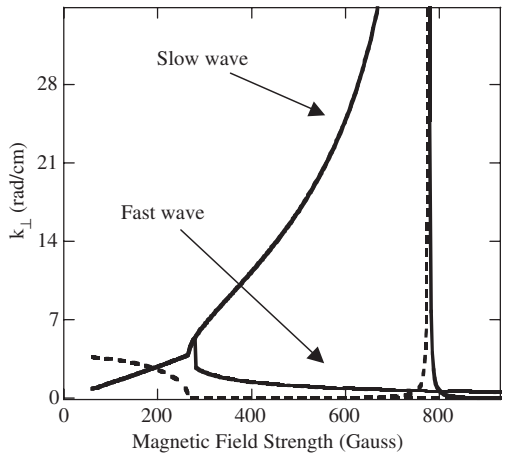

Figure 1. Solutions of the cold plasma dispersion relationship for $k_\perp$ with $n = 4 \times 10^{12}$ cm^{-3}, $k_{||} = 0.0785$ rad cm^{-1}, $f = 8$ MHz, and no collisions. (——) absolute value of real $k_\perp$ for the slow wave. (- - - -) absolute value of imaginary $k_\perp$ for the slow wave. (——) absolute value of real $k_\perp$ for the fast wave. (- - - -) absolute value of imaginary $k_\perp$ for the fast wave.

($B \sim 850$ G, $f_{RF} = 13.56$ MHz) lie to the left of the resonance in figure 1, i.e. they operate at RF frequencies well above the lower hybrid frequency.

2.1. Effects of plasma density

The slow wave solutions of the collisionless cold plasma dispersion relation as a function of magnetic field strength are shown in figure 2 for plasma densities of $n = 1 \times 10^{11}$ to 1×10^{13} cm^{-3}. For $n = 1 \times 10^{11}$ cm^{-3}, no resonant behaviour appears in the perpendicular wave number curve because such small densities reduce the lower hybrid frequency below 9 MHz for magnetic fields below 1400 G. Note that in equation (9), the ion plasma frequency term only affects the lower hybrid frequency at low plasma densities. In fact, low plasma densities reduce the lower hybrid frequency and matching the RF frequency to the lower hybrid frequency for $n = 1 \times 10^{11}$ cm^{-3} requires larger magnetic field strengths. For densities greater than 5×10^{11} cm^{-3} in HELIX, the ion plasma frequency term is only a small correction to the lower hybrid frequency. Thus, for a peaked density profile, the lower hybrid frequency at the plasma edge is lower than in the centre of the discharge.

The decrease in magnetic field strength required to match the RF frequency to the lower hybrid frequency due to increasing plasma density is also evident in calculations of the imaginary component of the perpendicular wave number shown in figure 2(*b*). The absolute value of the imaginary part of the wave number is greatest when the driving frequency is below the lower hybrid frequency, corresponding to heavy damping for slow waves with frequencies below the lower hybrid frequency. The magnitudes of the imaginary component are similar for all densities above 5×10^{11} cm^{-3}.

Because of the high-density, low-temperature nature of helicon sources, collisions can play a critical role in wave damping and resonant processes. Typically, the ion–ion and electron–electron collision frequencies are of the order of the RF frequency in helicon sources. When realistic collision frequencies are included in the calculations, equations (6)–(8), the resonance in the perpendicular wave number at the lower hybrid frequency for the slow wave becomes finite and the maximum value of both the real and imaginary parts is reduced (figure 3(*a*)). Not only is the maximum value of the perpendicular wave number reduced, the resonance frequency shifts to smaller magnetic field strengths and the width of the lower hybrid resonance increases [26]. The frequency shift due to collisions is easier to see if the denominators in equations (6)–(8) are converted to real values. The additional ν_j^2 term in each denominator is responsible for the changes in the resonant frequency for large collision frequencies. For the

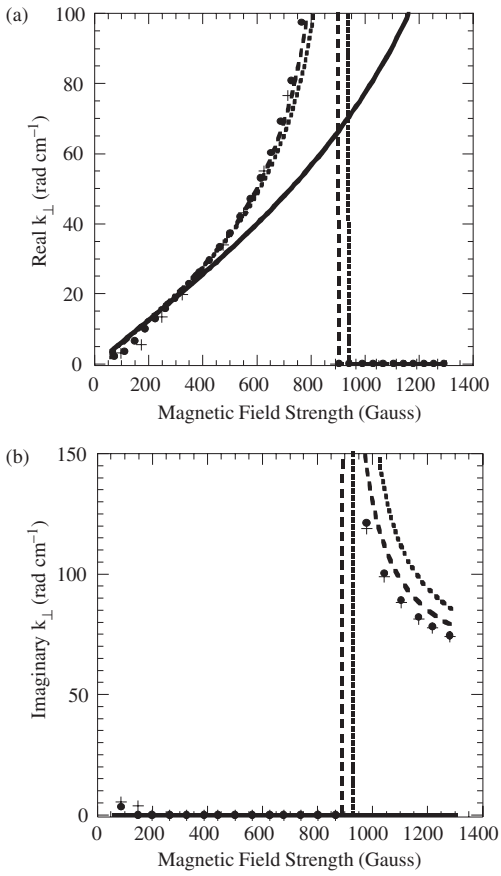

Figure 2. Absolute value of the (*a*) real and (*b*) imaginary components of $k_\perp$ for the slow wave with $k_{||} = 0.26$ rad cm^{-1}, $f = 9$ MHz, no collisions and densities of (——) $n = 1 \times 10^{11}$ cm^{-3}, (- - - -) $n = 5 \times 10^{11}$ cm^{-3}, (- - - -) $n = 1 \times 10^{12}$ cm^{-3}, (• • •) $n = 5 \times 10^{12}$ cm^{-3}, and (+ + +) $n = 1 \times 10^{13}$ cm^{-3} as a function of magnetic field strength.

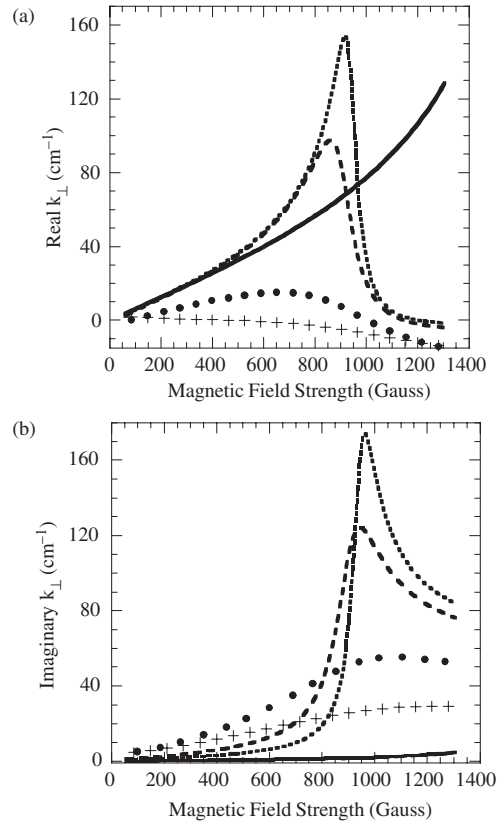

Figure 3. Absolute value of the (*a*) real and (*b*) imaginary components of $k_\perp$ for the slow wave with $k_{||} = 0.26$ rad cm^{-1}, $f = 9$ MHz, neutral pressure of 6.7 mTorr, electron temperature of 3 eV, ion temperature of 0.2 eV and plasma densities of (——) $n = 1 \times 10^{11}$ cm^{-3}, (- - - -) $n = 5 \times 10^{11}$ cm^{-3}, (- - - -) $n = 1 \times 10^{12}$ cm^{-3}, (• • •) $n = 5 \times 10^{12}$ cm^{-3}, and (+ + +) $n = 1 \times 10^{13}$ cm^{-3} as a function of magnetic field strength.

fast wave, collisions reduce the perpendicular wave numbers for the fast wave by 50%, but the resulting wave phase speeds are still too large to interact with thermal ions.

2.2. Effects of parallel wave number

The calculated perpendicular wave numbers for the slow wave for five different parallel wave numbers, ranging from $k_{||} = 0.01$ to $1.0\,\mathrm{cm}^{-1}$, for a plasma density of $5 \times 10^{12}\,\mathrm{cm}^{-3}$ and a RF frequency of 9 MHz are shown in figure 4(*a*) as a function of magnetic field strength. Although the magnetic field strength at which the lower hybrid resonance occurs remains constant, the magnitudes of both the real and imaginary components of the perpendicular wave number for the slow wave increase with increasing parallel wave number. Chen's calculations for both the fast and slow waves that included radial and axial boundaries, but not ion motion effects, showed similar increases in the perpendicular wave number for increasing parallel wave number [27]. Balkey [28] reported a sharp increase in edge parallel wave number for operational parameters that yielded the highest ion temperatures in the all Pyrex HELIX experiment. These calculations suggest that the perpendicular wave number also probably increased for those parameters and therefore the increased ion temperatures could have resulted from Landau damping of waves whose phase velocity had suddenly decreased to values close to the ion thermal speed.

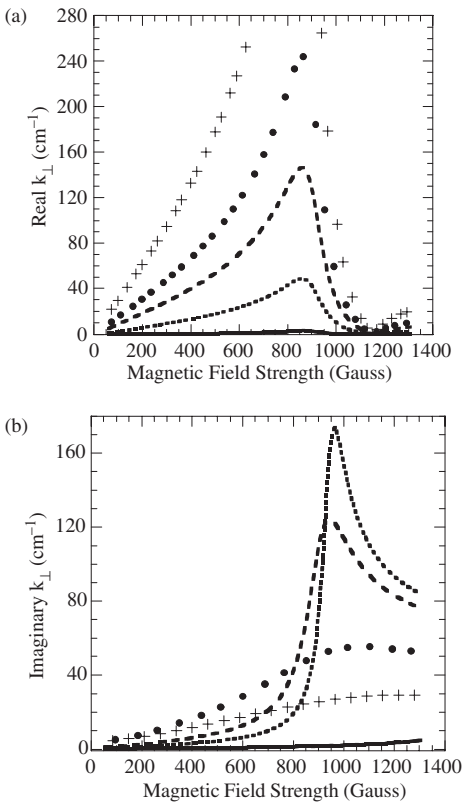

Figure 4. Absolute value of the (*a*) real and (*b*) imaginary components of $k_\perp$ for the fast wave versus magnetic field strength with $f = 9$ MHz, density of $5 \times 10^{12}\,\mathrm{cm}^{-3}$, neutral pressure of 6.7 mTorr, electron temperature of 3 eV, ion temperature of 0.2 eV, and parallel wave numbers of (——) $k_{||} = 0.01\,\mathrm{rad\,cm}^{-1}$, (- - - -) $k_{||} = 0.1\,\mathrm{rad\,cm}^{-1}$, (- - - -) $k_{||} = 0.3\,\mathrm{rad\,cm}^{-1}$, (• • •) $k_{||} = 0.5\,\mathrm{rad\,cm}^{-1}$, and (+ + +) $k_{||} = 1.0\,\mathrm{rad\,cm}^{-1}$.

2.3. Effects of RF frequency and magnetic field strength

In RF heating of tokamaks, lower hybrid wave heating has the advantage of being both density and magnetic field dependent. Therefore, lower hybrid heating is used to heat specific regions of the plasma [29]. Similar attempts have been made to control the density profile in plasma processing sources using the slow wave [30]. For ion heating, the location of the resonance in the plasma is not as important as the minimum perpendicular wave phase speed. For ion Landau damping in our experiment (HELIX), the minimum phase speed of the slow wave must be near the ion thermal speed, i.e. the perpendicular wave numbers must be large, $k_\perp > 150\,\mathrm{rad\,cm}^{-1}$. To determine for what RF frequencies and magnetic field strengths ion Landau damping could occur at some radial location in our experiment, the cold plasma dispersion relation was solved for a range of magnetic field strengths and RF frequencies. To account for the changing density as a function of radius, the calculations were performed for a range of densities corresponding to a typical density profile for each RF frequency and magnetic field strength combination. The maximum wave number as a function of plasma density, i.e. radial location, was then recorded.

Examples of such calculations for typical HELIX parameters are shown in figure 5. The maximum, normalized, real, perpendicular wave numbers for the slow wave, $k_\perp v_{\mathrm{thi}}/\omega$, are shown in figure 5(*a*) for magnetic fields of 500–1300 G and for RF frequencies from 7.5 to 15 MHz. The absolute values of the imaginary perpendicular wave numbers are shown in figure 5(*b*). Note that the peaks in the real and imaginary wave numbers occur at different combinations of RF frequency and magnetic field strength, i.e. the damping is not the strongest for the parameters at which the real part of the perpendicular wave number is the largest. This significance of this point will be revisited after the ion temperature measurements have been presented. Although the slowest wave phase speed is still roughly five times the ion thermal speed in figure 5, it is important to note that these calculations represent a lower (upper) bound on the perpendicular wave number (phase speed) of the slow wave. A relatively small decrease in the total collision frequency used in the calculations will dramatically increase (decrease) the calculated perpendicular wave number (phase speed) of the wave. Therefore, these calculations suggest that slow waves can ion Landau damp in our helicon plasmas.

To include the entire range of typical experimental helicon source parameters, the same calculations were also performed for a larger range of magnetic field strengths, 250–3300 G, and RF frequencies, 5–30 MHz, for two different plasma densities (figure 6). The decrease in the lower hybrid frequency due to the ion plasma frequency term is responsible for the nonlinear curve of the lower hybrid resonance in figure 6(*a*) (the boundary between the red and blue regions in figure 6(*a*)). If the ion plasma term was ignorable, the RF frequency at which the peak in the perpendicular wave number occurred would increase linearly with increasing magnetic field strength (as shown by the white line in the figure). The expected

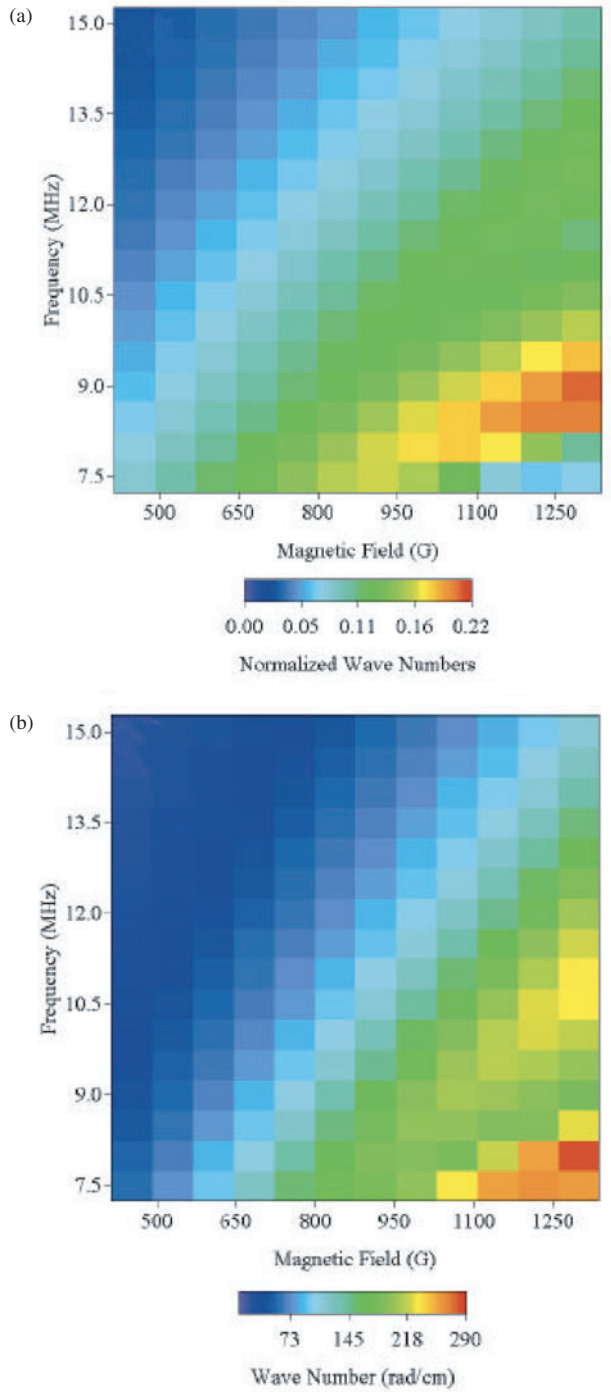

Figure 5. Maximum value of the (*a*) normalized ($v_{thi}k_{\perp}\omega$) real and (*b*) raw imaginary perpendicular wave number solution for the slow wave as a function of RF driving frequency and magnetic field strength for a peak density of 5×10^{12} cm^{-3}, a neutral pressure of 6.7 mTorr, electron temperature of 3 eV, ion temperature of 0.2 eV, and $k_{||}$ of 0.3 rad cm^{-1}.

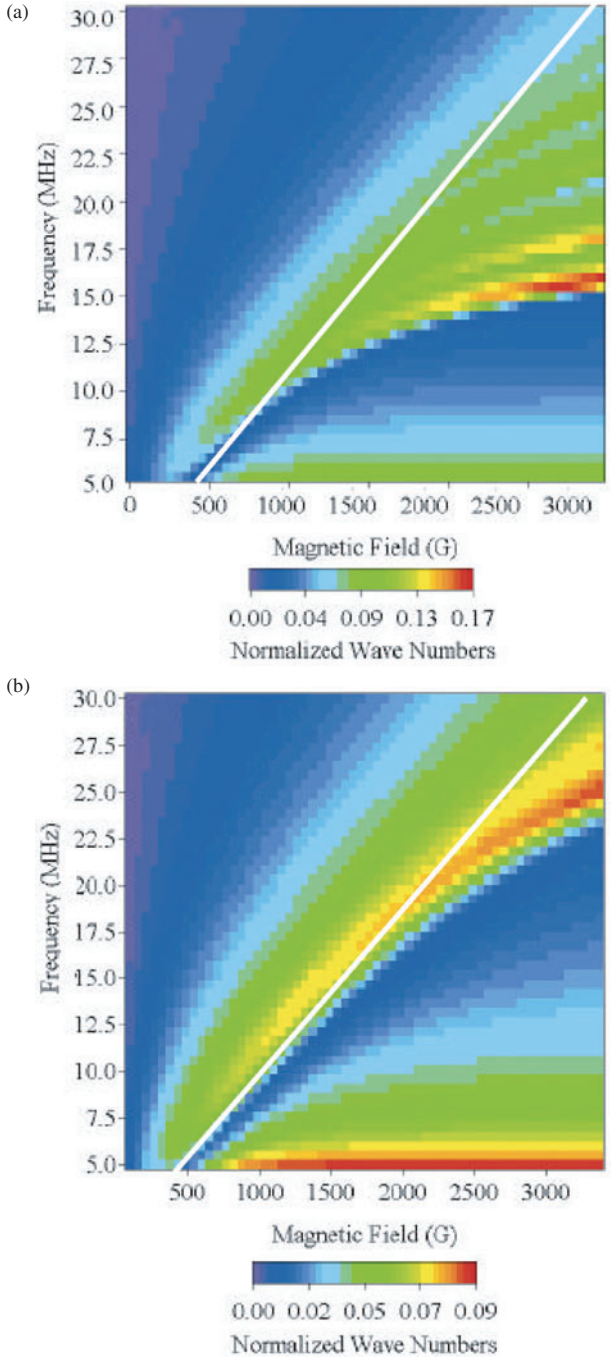

Figure 6. Maximum value of the normalized ($v_{thi}k_{\perp}/\omega$) real perpendicular wave number solution for the slow wave as a function of RF driving frequency and magnetic field strength for a peak density of (*a*) 5×10^{12} cm^{-3} and (*b*) 2×10^{13} cm^{-3} with a neutral pressure of 6.7 mTorr, electron temperature of 3 eV, ion temperature of 0.2 eV, and $k_{||}$ of 0.3 rad cm^{-1}.

linear relationship is evident in figure 6(*b*) as the peak plasma density was increased from 5×10^{12} to 2×10^{13} cm^{-3}. A key prediction of these calculations is that for a helicon source operating at 27 MHz, ion heating due to Landau damping of slow waves is unlikely to occur for low plasma densities and high magnetic field strengths. Note also that for helicon sources using argon, RF frequencies in the 7–30 MHz range, and magnetic field strengths of 400–3000 G, the lower hybrid frequency has a strong dependence on the plasma density as well as the magnetic field strength for densities less than 1×10^{13} cm^{-3}. For densities greater than 1×10^{13} cm^{-3}, the lower hybrid frequency depends almost exclusively on the magnetic field strength. Thus, the physics of low- and high-density helicon sources should differ substantially.

3. Experimental apparatus

The HELIX (figure 7) vacuum chamber is a 61 cm long, Pyrex tube 10 cm in diameter connected to a 91 cm long, stainless steel chamber that is 15 cm in diameter. The stainless steel chamber has one set of four 6″ Conflat™ crossing ports in the centre of the chamber and two sets of four $2\frac{3}{4}$″ Conflat™ crossing ports on either side that are used for diagnostic access. The opposite end of the stainless steel chamber opens into a 2 m diameter space simulation chamber, LEIA [10]. Ten electromagnets produce a steady-state axial magnetic field of 0–1200 G. The source gas is argon at neutral pressures of 1–10 mTorr. RF power of up to 2.0 kW over a frequency range of 6–18 MHz is used to create the steady-state plasma. A 19 cm, half wave, $m = +1$, helix antenna couples the RF energy into the plasma. Characteristic electron temperature and densities in HELIX are $T_e \approx 4$ eV and $n \geqslant 1 \times 10^{13}$ cm^3 as measured with an RF compensated Langmuir probe [31]. For all the experiments reported here, the magnetic field in LEIA was fixed at 36 G.

The ion temperatures, both parallel and perpendicular, were obtained from direct measurements of the ion velocity space distribution by laser induced fluorescence (LIF) [32, 33]. The LIF laser system consists of a 6 W Coherent Innova 300 argon ion laser that pumps a Coherent 899 tunable ring dye laser. At a wavelength of 611.5 nm, the laser pumps a metastable argon ion state to an upper state that then decays via emission of a 461.0 nm photon. As the laser frequency was varied over 10 GHz, the fluorescent emission from the pumped upper level was measured with a filtered photomultiplier tube detector. The filter in front of the photomultiplier has a 1 nm bandpass centred on the 461.0 nm emission line. The output of the dye laser was chopped at approximately 1 kHz and a reference signal from the chopper controller was sent to a Stanford Research SR830 lock-in amplifier that monitored the photomultiplier tube signal. The lock-in amplifier extracted the fluorescence signal from the intense background emission at the same wavelength. Typical LIF measurements using the lock-in amplifier had a signal-to-noise ratio of at least 20 : 1. After the laser light passed through the mechanical chopper, it was coupled into a fibre optic cable. The fibre optic cable transported the laser light from the laser laboratory into the helicon source laboratory where several sets of injection optics were mounted on the HELIX chamber. The collected fluorescence emission was also transported to the photomultiplier detector by fibre optic cable. This configuration allowed LIF measurements to be performed at different axial and radial locations in the plasma by moving the fibre optic cables. No other changes to the experimental hardware or data acquisition apparatus were required. For parallel injection, a linear polarizer-quarter wave plate combination was used to convert the unpolarized laser light exiting the fibre optic cable into circularly polarized light. With the laser light injected along the source axis of a single circular polarization, only one of the two $\sigma(\Delta m = +1)$ transitions was optically pumped. The much smaller internal Zeeman splitting of the σ lines was ignored during analysis of the parallel LIF data at magnetic field strengths under 1000 G.

Parallel and perpendicular ion temperature measurements were performed at the axial positions labelled A, B, and C in figure 7. At position A, 5 cm from the front of the antenna, the LIF measurements were performed at the centre of the discharge. The laser light (emission light) was injected (collected) through the wall of the Pyrex tube. At position B, 35 cm from the front of the antenna, the laser light (emission light) was injected (collected) through windows mounted on the small ports. For radial ion temperature profile measurements at position B, the injection optics were tilted to scan the measurement point along the plasma radius. At position C, 66 cm from the front of the antenna, a two-dimensional positioning system on motorized stages translated both the collection and injection optics to obtain two-dimensional ion temperature measurements.

For these experiments, two distinctly different magnetic field configurations were used. One configuration was a nearly uniform field using all ten electromagnets (ten-coil configuration) and the other included only the first eight electromagnets (eight-coil configuration). Although the last two electromagnets between HELIX and LEIA were disconnected in the eight-coil configuration, the maximum magnetic field strength increased because larger currents were possible with the voltage-limited power supply. Figure 8 shows

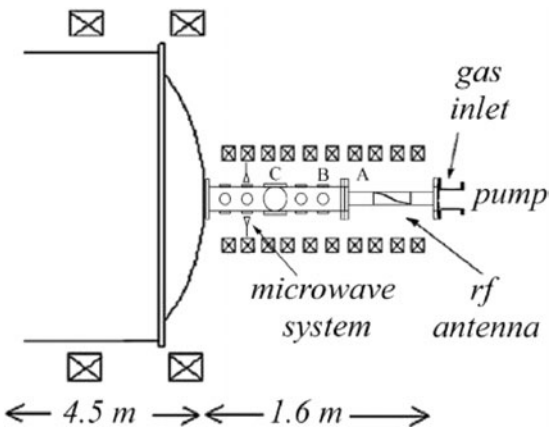

Figure 7. Schematic diagram of plasma chamber with diagnostic placement.

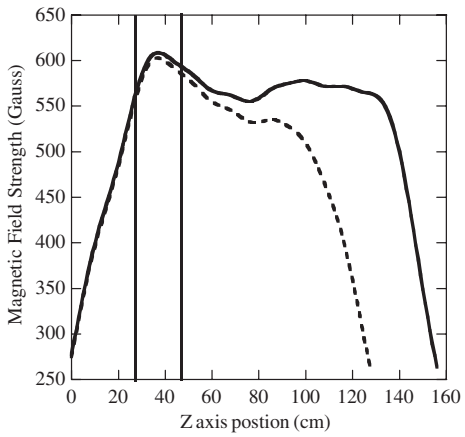

Figure 8. Axial magnetic field strength for (——) the ten-coil configuration and (- - - -) the eight-coil configuration in HELIX as a function of z with a current of 160 A in the HELIX magnets and 100 A in the LEIA magnets. The origin is at the edge of the Pyrex section at the end of the HELIX chamber. The two vertical lines represent the two ends of the antenna.

the axial magnetic strength profile for both configurations with the current in the HELIX magnets at 160 A. Note that the downstream magnetic field strength decreases faster in the eight-coil configuration.

4. Ion temperature measurements

In this section, experimental measurements of the ion temperature are shown for two different magnetic field configurations: the ten-coil configuration and the eight-coil configuration. For all measurements, the forward power to the antenna was held constant at 750 W with a deviation of less than 3% and the neutral pressure was fixed at 6.8 mTorr. The density range in the ten-coil configuration was $(0.1–0.75) \times 10^{12}$ cm^{-3} and peaked when the RF driving frequency was near the on-axis lower hybrid frequency. Similarly, the density range in the eight-coil configuration was $(0.1–3.0) \times 10^{12}$ cm^{-3} and again a density enhancement was observed when the RF driving frequency was near the on-axis lower hybrid frequency [17].

4.1. The ten-coil configuration

With all ten electromagnets, the maximum magnetic field strength in HELIX was 1125 G. Operating the source at RF frequencies lower than 8.5 MHz was problematic in the ten-coil configuration due to an inability to obtain a good antenna match, i.e. the capacitance in the matching circuit was insufficient to compensate for the inductance of the antenna and transmission line. The ten-coil configuration did have the advantage that the magnetic field lines at the edge of the plasma did not terminate on the conducting vacuum chamber wall in HELIX near the end of the source. This type of magnetic field geometry would correspond to helicon source models without conducting endplates.

Figure 9 shows the perpendicular ion temperature in the ten-coil configuration as a function of magnetic field strength and driving frequency for axial locations of 5, 35, and 65 cm from the antenna. The maximum perpendicular ion temperatures occur at the 35 cm location, indicating that the ion heating has a maximum downstream from the antenna. The peak in the ion heating downstream from the antenna is reminiscent of measurements of plasma density peaks downstream from the antenna in other helicon sources [34–36]. The peak in the perpendicular ion temperature downstream from the antenna also suggests that the parallel ion thermal conductivity in helicon sources is small compared to the radial diffusion time of the ions which is most likely due to the high ion–ion and ion–neutral collision frequency in the source.

Figures 9(*a*) and (*c*) do not suggest a strong dependence of ion temperature on driving frequency. However, the measurements shown in figure 9(*b*) demonstrate that the largest perpendicular ion temperatures occur for RF frequencies just above the on-axis lower hybrid frequency (the white line in figure 9). Although the perpendicular ion temperatures observed in these experiments are about half the maximum values reported by Balkey *et al* [16] for an all-glass vacuum chamber, they still exceed what would be expected for simple ion–electron thermal equilibration for realistic ion energy confinement times in HELIX [16].

A detailed examination of the perpendicular ion temperature suggests that the mechanism responsible for ion heating near the antenna is distinctly different than the downstream ion heating mechanism. Figure 10 shows the perpendicular ion temperature as function of magnetic field strength for an RF frequency of 9 MHz. At low magnetic field strengths, the perpendicular ion temperature near the antenna is actually higher than at the other locations. The peak in the downstream perpendicular ion temperature appears as the magnetic field strength increases. Note that the perpendicular ion temperature near the antenna decreases slightly with increasing magnetic field strength. The drop in temperature with increasing magnetic field strength does not occur at the other axial locations, suggesting that the ion heating mechanism near the antenna is fundamentally different than the ion heating mechanism at the other downstream locations.

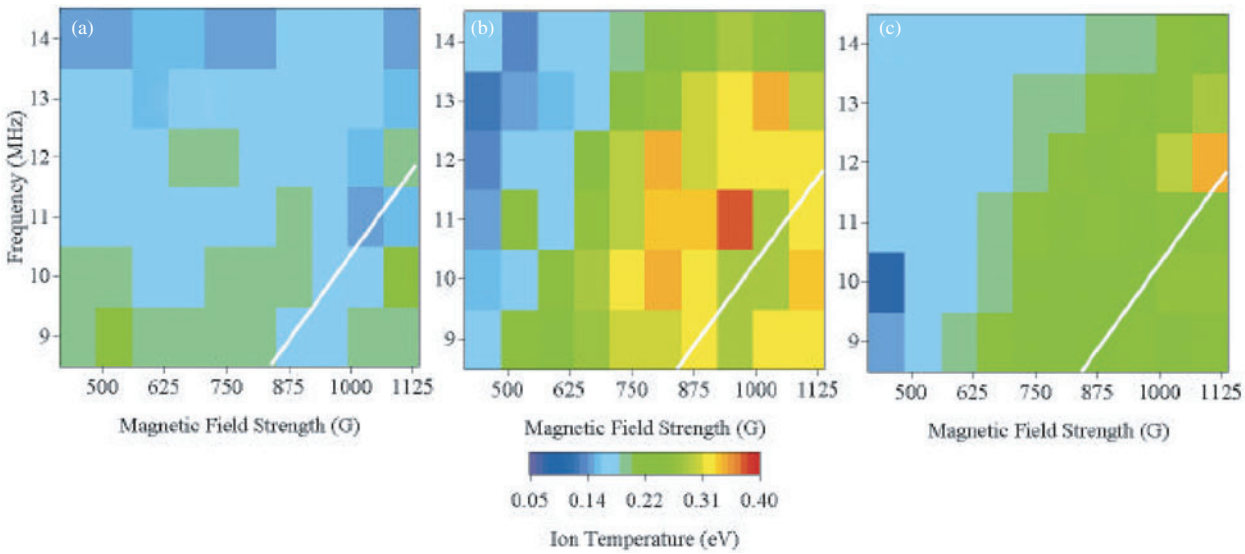

Figure 9. Perpendicular ion temperature versus driving (RF) frequency and magnetic field strength: (*a*) 5 cm from antenna, (*b*) 35 cm from antenna, and (*c*) 65 cm from antenna.

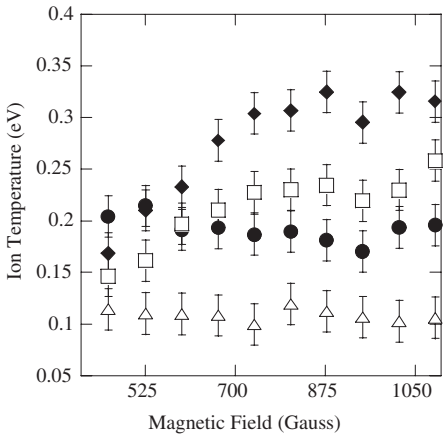

Figure 10. Perpendicular ion temperature versus magnetic field strength for four different axial locations measured from the front of the antenna: (△) −24 cm, (●) 5 cm, (♦) 35 cm, and (□) 65 cm.

Also shown in figure 10 is the perpendicular ion temperature on the upstream side of the antenna (−24 cm from the front of the antenna). The perpendicular ion temperature on the upstream side of the antenna is constant with increasing magnetic field strength and is lower than all three of the downstream locations. The difference in the ion temperatures upstream and downstream of the antenna clearly indicate directional coupling of the RF energy into the ions. The upstream ion temperatures are roughly what would be expected for ion–electron thermal equilibration due to ion–electron collisions.

Using the two-dimensional LIF system at the 65 cm axial location, the perpendicular ion temperature and the parallel ion temperature were measured as a function of radial position. Radial profiles of the perpendicular ion temperature are shown in figure 11(*a*) for four different magnetic field strengths. For the three lowest magnetic field strengths, there is a statistically significant trend of perpendicular ion temperature peaks on-axis and at the edge of the plasma. The parallel ion temperatures at the same four magnetic field strengths are shown in figure 11(*b*). As the magnetic field strength increases, the radial location of the peak parallel ion temperature shifts from roughly 1 cm at the lowest magnetic field strength to roughly 2.5 cm at the highest lowest magnetic field strength. Comparing the perpendicular and parallel ion temperatures at each of the four magnetic field strengths, the ion temperature anisotropy ($T_\perp/T_{||}$) ranges from $T_\perp/T_{||} \sim 1.9$ at the lowest magnetic field strength to $T_\perp/T_{||} \sim 1.3$ at the highest magnetic field strength. The variation in anisotropy is consistent with expectations for ion–ion thermalization given an increasing ion confinement time. Since the radial profile measurements are downstream ($z = 65$ cm) of the peak heating location ($z = 35$ cm), the ion distributions with the highest confinement times (largest magnetic field strengths) are the least anisotropic. Increasing confinement might also be responsible for the flattening of the radial ion temperature profiles with increasing magnetic field strength.

4.2. The eight-coil configuration

In the eight-coil configuration, the maximum magnetic field strength in HELIX increased to 1320 G. Apart from being able

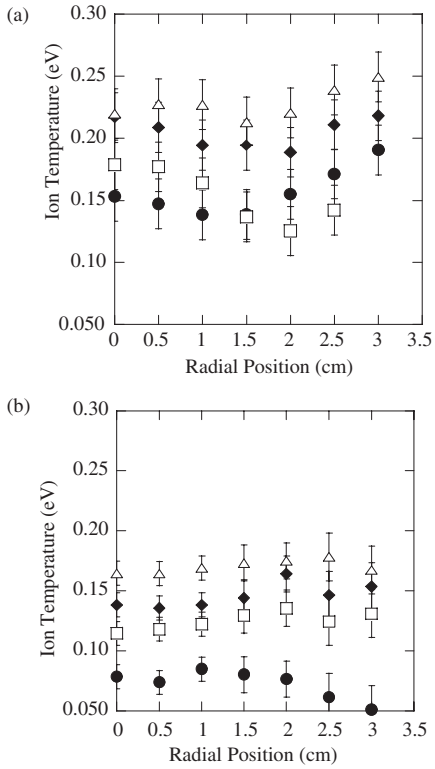

Figure 11. Radial variation of perpendicular (*a*) and parallel (*b*) ion temperature for four different magnetic field strengths: (●) 515 G, (□) 656 G, (♦) 868 G, and (△) 1080 G.

to match the antenna at frequencies as low as 7.5 MHz, the main difference between the eight- and ten-coil configurations is that in the eight-coil configuration, the magnetic field lines near the edge of the plasma intersect the conducting vacuum chamber wall just before the LEIA chamber while the inner magnetic field lines do not. The intersection of the magnetic field lines with the conducting chamber wall imposes a conducting axial boundary condition on the edge region of the plasma, thereby making the physical geometry of the edge of the plasma similar to the model used by Cho [19] in his study of lower hybrid resonance effects in helicon sources. The intersection of the edge magnetic field lines with a conducting boundary also occurred in the Balkey *et al* [16] experiments. In those experiments, a stainless steel bellows connected the Pyrex chamber to LEIA and the divergence of the magnetic field at the HELIX–LEIA interface resulted in the edge magnetic field line intersecting the conducting bellows. It is important to note that at all LIF measurement locations, the deviation of the magnetic field direction from the axial direction is too small to cause a significant mixing of perpendicular and parallel ion velocity components.

Perpendicular and parallel ion temperatures were measured at two different axial locations in the eight-coil configuration (figures 12 and 13). As in the ten-coil configuration, the perpendicular and parallel ion temperatures downstream from the antenna ($z = 35$ cm) are higher than in front of the antenna ($z = 5$ cm). Near the antenna ($z = 5$ cm), the ion temperatures have a small anisotropy on-axis, but downstream ($z = 35$ cm) the ion temperature is isotropic in the centre of the plasma. At the 35 cm

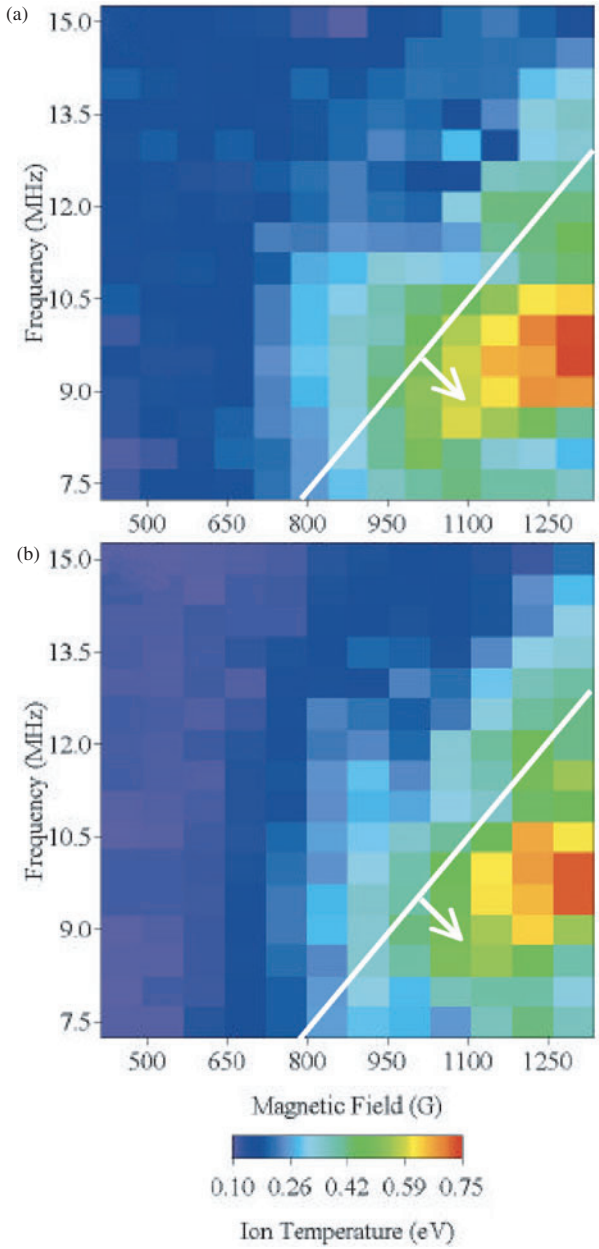

Figure 12. Ion temperature versus frequency and magnetic field in the (*a*) perpendicular and (*b*) parallel direction for $z = 35$ cm. The white line is where the RF driving frequency is equal to the on-axis lower hybrid frequency and the arrow points in the direction the line would move for lower plasma densities, i.e. at the edge of the plasma.

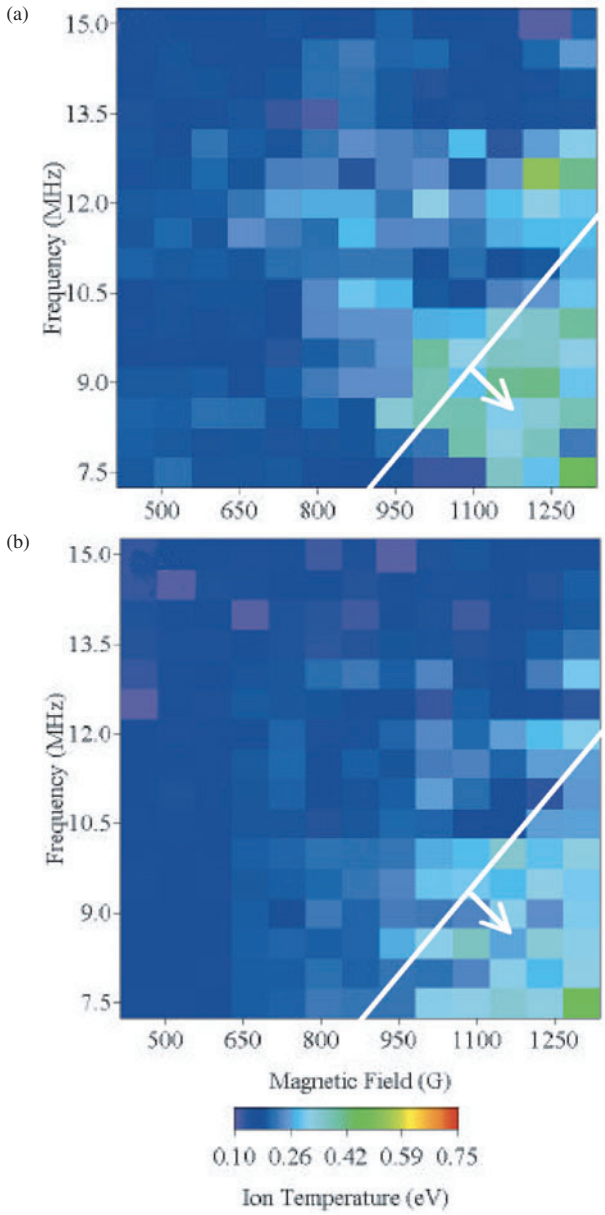

Figure 13. Ion temperature versus frequency and magnetic field in the (*a*) perpendicular and (*b*) parallel direction for $z = 5$ cm location. The white line is where the RF driving frequency is equal to the on-axis lower hybrid frequency and the arrow points in the direction the line would move for lower plasma densities, i.e. at the edge of the plasma.

location, the maximum perpendicular ion temperature is twice the maximum ion temperature observed in the ten-coil configuration and is comparable to the ion temperatures observed in the all Pyrex HELIX experiments [16]. The ion temperature measurements as a function of RF driving frequency and magnetic field strength at both locations clearly indicate a connection between ion heating and the lower hybrid frequency (figures 12 and 13). For RF frequencies below the on-axis lower hybrid frequency (shown by the solid white line in figures 12 and 13), the perpendicular and parallel temperatures at both locations are higher than for RF frequencies above the lower hybrid frequency. Although the shapes of the enhanced ion temperature regions are roughly similar at both locations, there are some significant differences. In the downstream ($z = 35$ cm) perpendicular ion temperature data (figure 12(*a*)), there is a well-defined peak, $T_i \sim 0.75$ eV, around an RF frequency of 9 MHz and the highest magnetic field strengths. Near the antenna ($z = 5$ cm), there is no such peak and for the lowest RF frequencies, less than 8.5 MHz, the perpendicular ion temperature does not increase for RF frequencies equal to the on-axis lower hybrid frequency (figure 13(*a*)). For low RF frequencies, the perpendicular ion temperature near the antenna and the parallel ion temperature downstream (figures 13(*b*) and 12(*b*)) increase only at the highest magnetic field strengths.

According to our calculations for slow wave propagation (the TG mode), slow waves excited at the edge of helicon sources are heavily damped by collisions and possibly by ion Landau damping as they propagate towards the centre of the plasma. Therefore, if slow waves play a role in coupling RF energy into the ions, the ion temperatures should be largest at the plasma edge. Perpendicular and parallel ion temperature profile measurements at $z = 35$ cm in both the perpendicular and parallel directions for three different sets of RF frequencies and magnetic field strengths are shown in figure 14. Each set of RF frequency and magnetic field strength combinations corresponds to a different ion temperature region in figure 12.

At a high RF frequency (13 MHz) and low magnetic field strength (571 G), low ion temperatures are observed and are independent of radial location (figure 14). These parameters correspond to an RF frequency well above the on-axis lower hybrid frequency. There is a small decrease in parallel ion temperatures with increasing radius from 0.11 eV on-axis to 0.08 eV towards the edge of the plasma. The parallel ion temperatures are three to four times room temperature and could result from either thermalization of the perpendicular ion temperature by ion–ion collisions or ion heating resulting from electron–ion collisions [16]. The perpendicular ion temperatures are well above room temperature and cannot be explained by electron–ion thermal collisional equilibration [16].

At an RF frequency of 10.5 MHz and a magnetic field strength of 878 G, low ion temperatures are observed and are again independent of radial location (figure 14). These parameters correspond to an RF frequency comparable to the on-axis lower hybrid frequency. The parallel ion temperatures also decrease slightly with increasing radius.

At an RF frequency of 9 MHz and a magnetic field strength of 1185 G, the perpendicular ion temperatures are constant in the centre of the source and increase sharply at the edge of the plasma (figure 14). These parameters correspond to an RF frequency much less than the on-axis lower hybrid frequency (the hot perpendicular ion temperature region seen in figure 12(*a*)). The increase in perpendicular ion temperature at the edge of the source is larger than the experimental error in the measurement and is reproducible. The parallel ion temperatures are peaked on-axis and decrease by 50% towards the edge of the plasma. The fact that the perpendicular and parallel ion temperatures are equal where the plasma density is the greatest suggests that thermal equilibration of the ions (due to ion–ion collisions) is responsible for heating the ions in the parallel direction. Towards the edge, the plasma density drops and ion confinement is poorer. Thus, the parallel ion temperature decreases towards the edge.

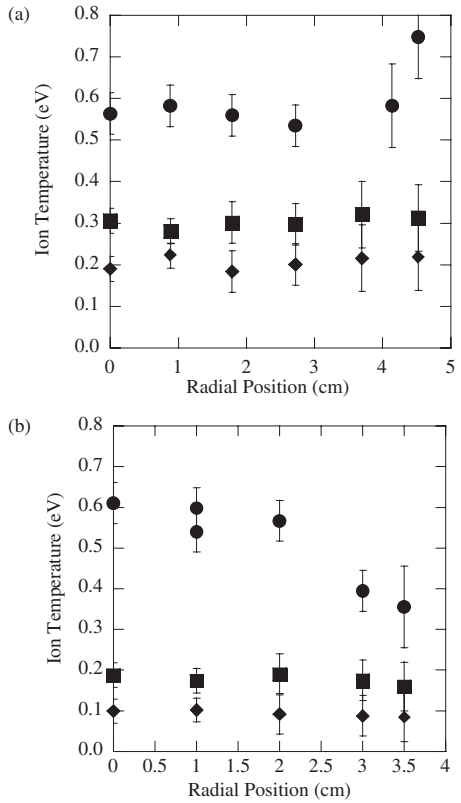

Figure 14. (*a*) Perpendicular and (*b*) parallel ion temperature versus radius for RF frequencies and magnetic fields combinations of (♦) 13 MHz and 571 G, (■) 10.5 MHz and 878 G, and (●) 9 MHz and 1185 G with a neutral pressure = 6.7 mTorr and RF power = 750 W.

5. Discussion

At large perpendicular wave numbers, the perpendicular phase speed of the slow wave, $\omega/k_\perp$, can be comparable to the ion thermal speed. Under these circumstances, the ions can Landau damp the slow wave, thereby gaining energy. Since the ion Landau damping occurs along the perpendicular direction, the ions will be preferentially heated in the perpendicular direction. The simple slow wave model presented in section 2 confirmed that the perpendicular wave number of the slow wave in HELIX can become large enough for ion Landau damping to occur. Because density profile effects shift the lower hybrid resonance towards the plasma edge (see section 2), ion heating due to Landau damping of the slow wave should occur near the edge of the plasma.

Ion temperature measurements in both the ten- and the eight-coil configuration clearly indicate perpendicular ion heating at the plasma edge (figures 11 and 14). The perpendicular ion temperatures can be radially uniform in the centre of the discharge only if the perpendicular ion heating occurs off-axis or if the ion thermal conductivity along the magnetic field is large enough to balance on-axis ion heating. Otherwise, cross-field diffusion would create a peaked ion temperature profile. The strong gradient in perpendicular ion temperature (figure 9) argues against a high ion thermal conductivity along the magnetic field. Therefore, the flat centre and peaked edge of the perpendicular ion temperature radial profile in the maximum heating case (figure 14) are strong evidence of edge perpendicular ion heating in the helicon source.

Close investigation of the differences in the ion temperature along the magnetic field has also revealed additional evidence in support of the slow wave, ion heating hypothesis. Subtraction of the perpendicular ion temperature near the antenna from the measurements at the $z = 35$ cm location provides a measure of the additional ion heating occurring downstream of the antenna. The difference in perpendicular ion temperature in the ten-coil configuration is shown in figure 15(*a*) as a function of RF driving frequency

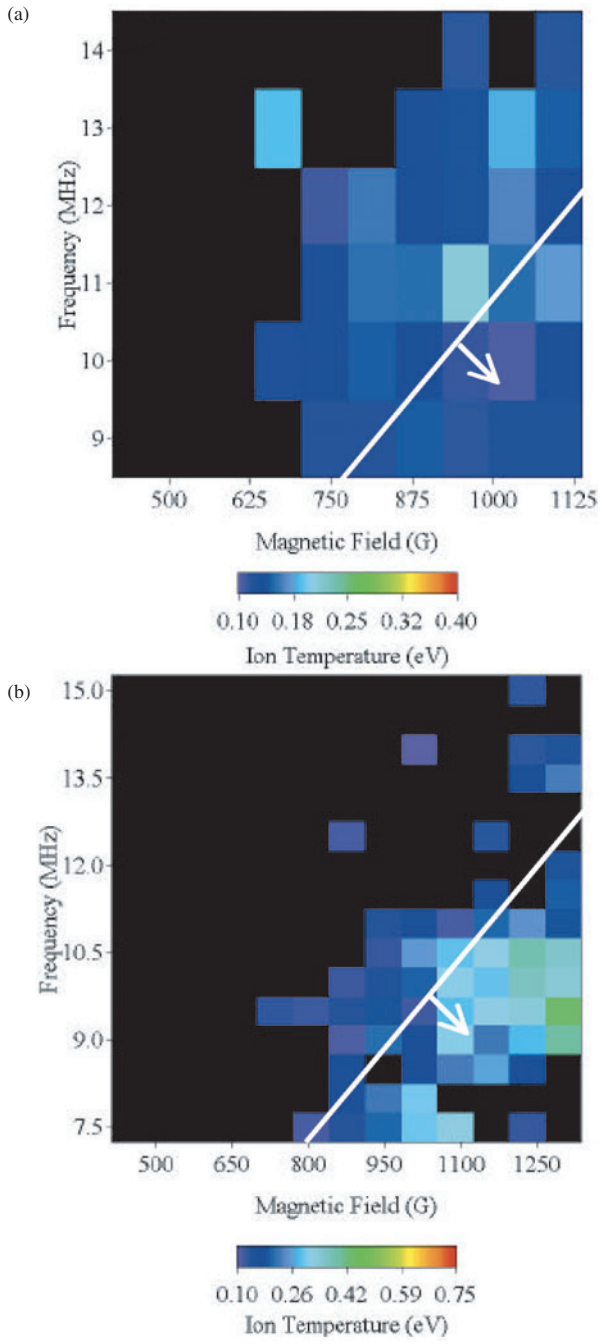

Figure 15. Difference in the perpendicular ion temperature at the $z = 35$ cm and $z = 5$ cm locations in the (*a*) ten-coil and in the (*b*) eight-coil configuration.

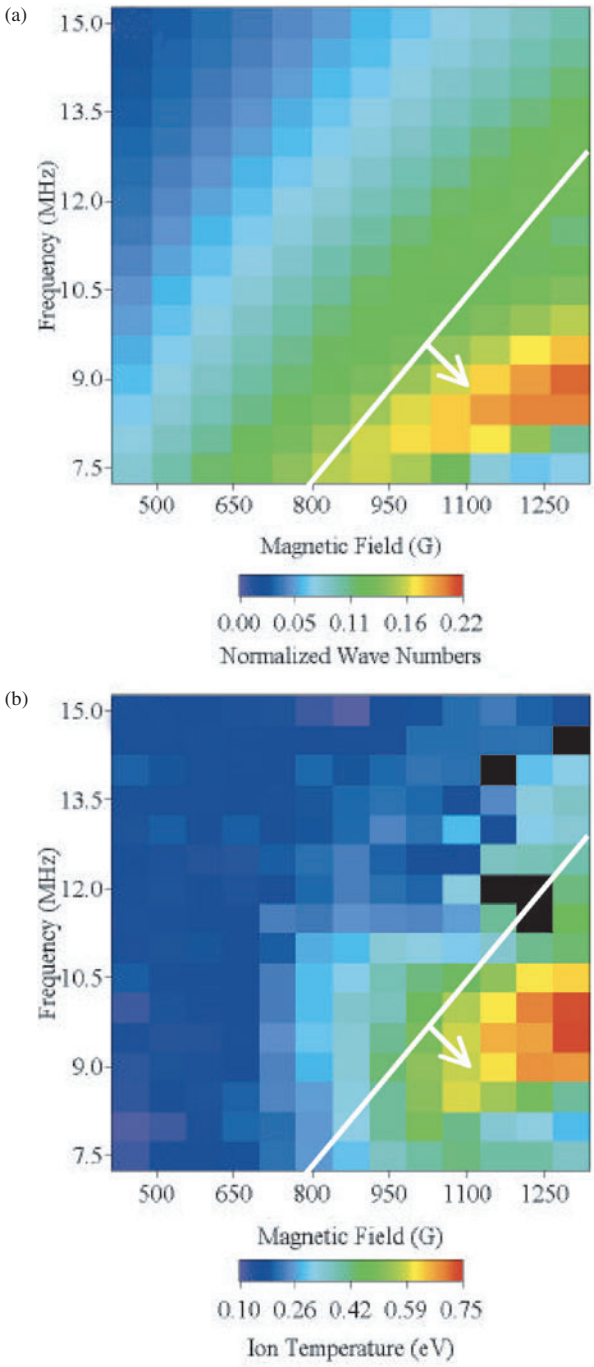

Figure 16. (*a*) Normalized ($v_{\mathrm{thi}} k_\perp \omega$) perpendicular wave numbers for slow wave model, (*b*) ion temperatures measured at the 35 cm location. The white line is where the RF driving frequency is equal to the on-axis lower hybrid frequency and the arrow points in the direction the line would move for lower plasma densities, i.e. at the edge of the plasma.

and magnetic field strength. The ion temperature difference is a maximum when the RF frequency is near or just below the on-axis lower hybrid frequency (figure 15(*a*)). Apart from the general correlation with lower hybrid frequency, there are no other distinct features in the temperature difference data.

The perpendicular ion temperature data from the eight-coil configuration, however, tell a remarkably different story. The perpendicular ion temperature difference in the eight-coil configuration is shown in figure 15(*b*) as a function of RF driving frequency and magnetic field strength. There is still a strong correlation between additional ion heating and when the RF frequency is below the lower hybrid frequency (the white line in figure 15(*b*) indicates where the RF driving frequency matches the on-axis lower hybrid frequency), but in the eight-coil configuration a distinct peak in the downstream perpendicular ion temperature appears around an RF frequency of 9.5 MHz and a magnetic field strength of 1200 G.

In figure 16, the normalized perpendicular wave numbers, $k_\perp v_{\mathrm{thi}}/\omega$, calculated with the simple model described in

section 2 for the experimental parameters of these experiments are plotted versus RF frequency and magnetic field strength. For comparison, the perpendicular ion temperature differences shown in figure 15(*b*) are plotted again in figure 16(*b*). Both the broad trends and the location of the peaks in figures 16(*a*) and (*b*) are quantitatively consistent. Where the model predicts the largest perpendicular wave numbers, the downstream ions are most strongly heated in the perpendicular direction. Where the model predicts a decrease in wave number at low RF frequency and high magnetic field strength, the ion perpendicular ion temperatures are correspondingly low. Although the model predicts peak values for the normalized wave numbers of the order of 0.2, i.e. phase speeds about five times the ion thermal speed, Landau damping of waves with comparable phase to thermal speed ratios has been observed in other experiments [25].

Note also that the shift in the ion temperature peak towards RF frequencies and magnetic field strengths such that the RF frequency is well below the on-axis lower hybrid frequency is easily explained just in terms of damping of slow waves at the lower hybrid resonance. If the plasma density is low enough, the ion plasma frequency term becomes important in the calculation of the lower hybrid frequency. On-axis, the plasma density is much higher and cyclotron term, $\omega_{ce}\omega_{ci}$, dominates. Therefore, towards the edge of the plasma where the density decreases, the ion plasma frequency term serves to lower the actual lower hybrid frequency. The arrow in figure 16 shows to what values of RF frequency and magnetic field strength, the resonance condition will shift in the plasma edge. If the perpendicular ion heating results of damping of the slow wave at the lower hybrid resonance, the maximum ion heating should occur at RF frequencies and magnetic field strengths such that the RF frequency is below the on-axis lower hybrid frequency because the slow wave only exists in the plasma edge [22, 27, 37]. Thus, the RF frequencies and magnetic field strengths at which the maximum perpendicular ion heating occurs support the conclusion that damping of the slow wave plays a key role in downstream ion heating in helicon sources.

6. Conclusions

Theoretical studies over the past decade have suggested that coupling to and subsequent damping of the slow wave could explain the high RF absorption efficiency of the helicon source [14, 37, 38]. To date, no direct measurements of the slow wave have been accomplished. Recent experimental measurements of large axial currents at the RF frequency in the edge of a helicon source provide evidence of slow wave excitation [24]; however, the wave fields of the slow wave have not been directly measured in any helicon source. The downstream perpendicular ion temperature measurements presented in this work are consistent with the excitation and damping of slow waves at the edge of the plasma. The perpendicular ion temperature is a maximum when the RF frequency matches the lower hybrid frequency at the plasma edge; only the slow wave has a resonance at the local lower hybrid frequency. The perpendicular ion temperature is largest at the edge of the plasma; only the slow wave propagates at the plasma edge as the density is too low for helicon wave propagation. The ion temperatures are low enough that extremely low phase speed waves are required for direct wave–particle interactions that could result in ion heating; only the perpendicular wavelengths of the slow wave are large enough near the lower hybrid resonance to yield low very low phase speed waves. In fact, the perpendicular wavelengths of the slow wave near resonance are smaller than or equal to the ion mean free path. Thus, ions can exchange momentum with slow waves even though the plasma is highly collisional. The only definitive way to prove the existence of the slow wave would be to directly measure the short wavelength, slow wave fluctuations. Laser scattering methods [39] can measure the large perpendicular wave numbers, $k_\perp \geqslant 100\,\mathrm{rad\,cm^{-1}}$ or $\lambda \leqslant 1$ mm, undetectable with probes. As yet, no such measurements have been made in helicon sources. However, recent microwave scattering experiments in a helicon source have detected somewhat longer wavelength fluctuations, $\lambda > 1$ mm, confirming that wave scattering experiments can be accomplished in helicon sources [40]. Until such measurements are made, these perpendicular ion temperature measurements provide the most conclusive evidence to date of the excitation and damping of slow waves in helicon sources.

Acknowledgments

This work was performed with support from the National Science Foundation under grant ATM-99988450 and the US Department of Energy under grant DE-FG02-97ER54420.

References

[1] Perry A J, Vender D and Boswell R W 1991 *J. Vac. Sci. Technol.* B (*Microelectron. Process. Phenomena*) **9** 310
[2] Okamoto N, Kasahara F and Ikoma H 1999 *Japan. J. Appl. Phys.* (Part 2) (*Letters*) **38** L424
[3] Chen F F, Jiang X and Evans J D 2000 *J. Vac. Sci. Technol.* A **18** 2108
[4] Chen F F 1992 *J. Vac. Sci. Technol.* A **10** 1389
[5] Hershkowitz N, Ding J, Breun R A, Chen R T S, Meyer J and Quick A K 1996 *Phys. Plasmas* **3** 2197
[6] Chang Diaz F R *et al* 1999 *Fusion Technol.* **35** 243
[7] Cohen S A *et al* 1999 *Bull. Am. Phys. Soc.* **44** 238
[8] Light M, Chen F F and Colestock P L 2001 *Phys. Plasmas* **8** 4675
[9] Light M E 2000 *PhD Dissertation* University of California, Los Angeles, USA
[10] Scime E E, Keiter P A, Balkey M M, Bolvin R F, Kline J L, Blackburn M and Gary S P 2000 *Phys. Plasmas* **7** 2157
[11] Scime E E, Keiter P A, Zintl M W, Balkey M M, Kline J L and Koepke M E 1998 *Plasma Sources Sci. Technol.* **7** 186
[12] Hanna J and Watts C 2001 *Phys. Plasmas* **8** 4251
[13] Keiter P A, Scime E E, Balkey M M, Boivin R, Kline J L and Gary S P 2000 *Phys. Plasmas* **7** 779
[14] Arnush D 2000 *Phys. Plasmas* **7** 3042
[15] Shamrai K P and Taranov V B 1995 *Phys. Lett.* A **204** 139
[16] Balkey M M, Boivin R F, Kline J L and Scime E E 2001 *Plasma Sources Sci. Technol.* **10** 284
[17] Kline J L, Scime E E, Boivin R F, Keesse A and Sun X 2002 *Phys. Rev. Lett.* **88** 195002
[18] Davies B 1970 *J. Plasma Phys.* **4** 43
[19] Cho S 2000 *Phys. Plasmas* **7** 417
[20] Boswell R W 1984 *Plasma Phys. Control. Fusion* **26** 1147
[21] Light M, Sudit I D, Chen F F and Arnush D 1995 *Phys. Plasmas* **2** 4094
[22] Chen F F and Arnush D 1997 *Phys. Plasmas* **4** 3411
[23] Yun S, Suwon C, Tynan G and Hongyoung C 2001 *Phys. Plasmas* **8** 358

[24] Blackwell D D, Madziwa T G, Arnush D and Chen F F 2002 *Phys. Rev. Lett.* **88** 145002
[25] Wong K L and Ono M 1981 *Phys. Rev. Lett.* **47** 842
[26] Yun S M and Chang H Y 1998 *Phys. Lett.* A **248** 400
[27] Arnush D and Chen F F 1997 *Phys. Plasmas* **4** 3411
[28] Balkey M M 2000 *PhD Dissertation* West Virginia University, Morgantown, USA
[29] Stix T H 1965 *Phys. Rev. Lett.* **15** 878
[30] Kikuchi T, Onnishi K, Yasaka Y, Tachibana K and Itoh T 1999 *Japan. J. Appl. Phys.* (Part 1) (*Regular Papers, Short Notes & Review Papers*) **38** 4351
[31] Sudit I D and Chen F F 1994 *Plasma Sources Sci. Technol.* **3** 162
[32] Stern R A and Johnson J A III 1975 *Phys. Rev. Lett.* **34** 1548
[33] Hill D H, Fornaca S and Wickham M G 1983 *Rev. Sci. Instrum.* **54** 309
[34] Sudit I D and Chen F F 1996 *Plasma Sources Sci. Technol.* **5** 43
[35] Chen F F 1996 *Phys. Plasmas* **3** 1783
[36] Chen F F and Boswell R W 1997 *IEEE Trans. Plasma Sci.* **25** 1245
[37] Shamrai K P and Taranov V B 1996 *Plasma Sources Sci. Technol.* **5** 474
[38] Cho S 1996 *Phys. Plasmas* **3** 4268
[39] Wurden G A, Wong K L and Ono M 1985 *Phys. Fluids* **28** 716
[40] Kaganskaya N M, Krämer M and Selenin V L 2001 *Phys. Plasmas* **8** 4694